

Cosmological production of H_2 before the formation of the first galaxies

Christopher M. Hirata¹ and Nikhil Padmanabhan²

¹*School of Natural Sciences, Institute for Advanced Study, Einstein Drive, Princeton, NJ 08540, USA*

²*Joseph Henry Laboratories, Department of Physics, Jadwin Hall, Princeton University, Princeton, NJ 08544, USA*

3 August 2021

ABSTRACT

Previous calculations of the pregalactic chemistry have found that a small amount of H_2 , $x[\text{H}_2] \equiv n[\text{H}_2]/n[\text{H}] \approx 2.6 \times 10^{-6}$, is produced catalytically through the H^- , H_2^+ , and HeH^+ mechanisms. We revisit this standard calculation taking into account the effects of the nonthermal radiation background produced by cosmic hydrogen recombination, which is particularly effective at destroying H^- via photodetachment. We also take into consideration the non-equilibrium level populations of H_2^+ , which occur since transitions among the rotational-vibrational levels are slow compared to photodissociation. The new calculation predicts a final H_2 abundance of $x[\text{H}_2] \approx 6 \times 10^{-7}$ for the standard cosmology. This production is due almost entirely to the H^- mechanism, with ~ 1 per cent coming from HeH^+ and ~ 0.004 per cent from H_2^+ . We evaluate the heating of the diffuse pregalactic gas from the chemical reactions that produce H_2 and from rotational transitions in H_2 , and find them to be negligible.

Key words: cosmology: theory – intergalactic medium – molecular processes.

1 INTRODUCTION

One of the key problems in cosmology is to understand the physical and chemical state of the baryonic matter in the Universe. At high redshift, the baryonic matter was fully ionized and co-existed with a thermalized radiation field (the cosmic microwave background, or CMB). By redshift $z \sim 10^3$, the Universe had expanded and cooled to ~ 3000 K, at which point the ionized nuclei and free electrons of the primordial plasma combined to form neutral atoms. This cosmic recombination was first studied theoretically by Peebles (1968) and Zel'dovich et al. (1968). The observations of the acoustic peaks in the CMB TT and TE power spectra (Lee et al. 2001; Netterfield et al. 2002; Halverson et al. 2002; Kogut et al. 2003; Page et al. 2006; Hinshaw et al. 2006) provide direct evidence that cosmic recombination happened, and that it occurred over a narrow range in redshift, in accordance with predictions.

As the Universe continued to expand and cool, the formation of molecules became thermodynamically favourable. Since hydrogen is most abundant, one would expect the most abundant molecule to be H_2 . However, unlike atomic recombination, which occurs shortly after it becomes thermodynamically favourable and proceeds nearly to completion (e.g. Seager et al. 2000), cosmological formation of molecules is slow and freezes out with a final abundance, $x[\text{H}_2] \equiv n[\text{H}_2]/n[\text{H}] \ll 1$.

Despite their small abundance, molecules in the early universe have been investigated for several reasons. The first is that the primordial gas, mainly of hydrogen and helium atoms, lacks the low-lying excitations necessary for cooling and therefore star formation at low temperatures. On the other hand, molecules (which possess low-lying rotational excitations) could provide the cooling necessary to form the first stars (Saslaw & Zipoy 1967). However, recent calculations indicate that the primordial H_2 abundance is far too small for this, and that the only H_2 important for cooling of early haloes is formed in collapsed haloes (e.g. Tegmark et al. 1997). A second reason for studying H_2 production is that the heating of the gas, either via rotational transitions induced by the CMB or the chemical energy released by formation of the molecules, could affect the temperature of the pregalactic gas. Here even a small effect could be important for proposals to study the absorption of the CMB by pregalactic gas in the $\text{H} \text{ I}$ 21-cm line (Loeb & Zaldarriaga 2004). Finally, there is the (perhaps academic) motivation to understand the composition of the primordial gas as part of elucidating the standard cosmological model.

The first calculation of the primordial H_2 abundance was by Saslaw & Zipoy (1967). Noting that the direct radiative association of two H atoms is forbidden, they proposed that H_2 molecules could be built up using H_2^+ as

arXiv:astro-ph/0606437v1 19 Jun 2006

an intermediate state (the specific reactions will be given in Section 2). Peebles & Dicke (1968) and Hirasawa et al. (1969) suggested that the H^- mechanism dominated the production of molecules in primordial gas clouds. A number of subsequent studies considered in increasing detail the H_2 abundance and cooling in primordial clouds (Hirasawa 1969; Yoneyama 1972; Hutchins 1976). Lepp & Shull (1984) performed a calculation of the abundances of H_2 as well as HD and LiH, calculating a final abundance $x[\text{H}_2] \sim 10^{-6}$ in the intergalactic gas. This is essentially today’s “standard” calculation of the primordial H_2 abundance, although some of the reaction rates and cosmological parameters have been updated. These updated analyses, which include substantial revisions to the deuterium and lithium chemistry, can be found in Puy et al. (1993), Palla et al. (1995), Galli & Palla (1998), Stancil et al. (1998), and references therein.

The effect of H_2 on heating of the gas before collapse has also been considered. Puy et al. (1993) presented the first analysis of the thermal effect of molecules; they found a moderate effect (~ 10 per cent) on the gas temperature mainly due to rotational lines in H_2 , and a smaller effect due to chemical reactions. The heating in rotational lines was also considered by Haiman et al. (1996a) and Galli & Palla (1998), but was revised downward by Flower & Pineau des Forêts (2000), who concluded the effect was insignificant. We revisit the chemical heating here, and conclude that it dominates over H_2 rotational lines. However, even this effect is probably too small to be detected by 21-cm experiments in the foreseeable future as it changes the gas temperature at the $\sim 10^{-4}$ level.

All of these analyses, however, have been based on several common assumptions. One is the assumption of a purely thermal radiation field, which is not completely correct because of the line and continuum radiation emitted during hydrogen and helium recombination (e.g. Rybicki & Dell’Antonio 1993; Wong et al. 2006). Indeed, Switzer & Hirata (2005) found that this spectral distortion suppresses the lithium abundance by several orders of magnitude as compared with previous calculations (Stancil et al. 1996; Galli & Palla 1998; Stancil et al. 2002). The other assumption is the use of H_2^+ photodissociation rates based either on local thermodynamic equilibrium (LTE) populations of the rotational-vibrational levels, or with all H_2^+ ions in the ground state. It is however known that H_2^+ forms preferentially in excited states and since radiative transitions between levels are slow, LTE may not apply. The importance of this was recognized by Galli & Palla (1998) and Lepp et al. (2002), but a full non-LTE analysis of H_2^+ level populations has not been done.

Our purpose here is to revisit the calculation of H_2 abundance, including spectral distortions to the CMB and with a level-resolved treatment of H_2^+ . In Section 2, we introduce the chemical reactions important for H_2 production. The H^- mechanism, including the effect of the spectral distortion, is discussed in Section 3. The H_2^+ mechanism and the level-resolved treatment is in Section 4, and HeH^+ is discussed in Section 5. The abundances of H_2 , H^- , H_2^+ , and HeH^+ are calculated for our presently favoured cosmology in Section 6. The heating of the pregalactic gas by H_2 and the chemical reactions leading to its formation is considered in Section 7. We conclude in Section 8. The theory of the

energy levels and transitions of the H_2^+ ion is recapitulated in Appendix A.

In this paper, we have assumed a primordial helium abundance of $Y_{\mathcal{P}} = 0.24$, and a flat Λ CDM cosmology with parameters from Seljak et al. (2005): $\Omega_b = 0.0462$, $\Omega_m = 0.281$, and $H_0 = 71.0 \text{ km s}^{-1} \text{ Mpc}^{-1}$. The number density n will refer to the total proper density of hydrogen nuclei in all forms (ionized, atomic, and molecular), although in the regime of interest here it is mostly atomic. The notation x_i (or $x[i]$ for H^- , H_2^+ , and HeH^+) will denote the number density of species i relative to the total number density of hydrogen nuclei in all chemical forms (e.g. $x[\text{H}_2] = n[\text{H}_2]/n = 1/2$ if all hydrogen is molecular).

2 THE REACTIONS

Due to the lack of a dipole moment, it is forbidden for two H atoms to combine radiatively to form H_2 . Therefore cosmological H_2 production proceeds through two main mechanisms catalyzed by charged particles (Saslaw & Zipoy 1967; Peebles & Dicke 1968; Hirasawa 1969). The H^- mechanism begins with radiative attachment to form H^- ,



and is completed when the associative detachment reaction



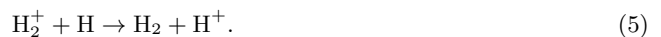
A minor reaction that can use up H^- ions is mutual neutralization,



An alternative mechanism is via H_2^+ , in which the catalyst is a proton rather than an electron,



The H_2^+ ion can then be converted to H_2 via the reaction



It is also possible for H_2^+ to be destroyed by dissociative recombination,



A third route is via the HeH^+ mechanism. This is unimportant in the “standard” calculation, but given that we are revising the H^- and H_2^+ rates downward it is only prudent to include it. It begins with the production of HeH^+ by radiative association,



This ion could either be photodissociated (reverse of Eq. 7), but it could also form H_2^+ by the reaction



The H_2^+ ion then participates in the usual sequence of reactions, Eqs. (4–6).

All three of these mechanisms are suppressed at high redshift due to the intense CMB radiation, which drives Eqs. (1), (4), and (7) strongly to the left. They are also inefficient at low redshift because the collisions required for them to proceed become rare as the universe expands and the gas density drops. Past calculations have H_2 production

peaking at $z \sim 260$ for the H₂⁺ mechanism and $z \sim 90$ for the H⁻ mechanism (e.g. Lepp et al. 2002).

Once formed, the H₂ molecule can be destroyed by UV photodissociation (Stecher & Williams 1967; Abgrall et al. 1992; Haiman et al. 1996b). Photoexcitation of H₂ from the ground $X^1\Sigma_g^+$ electronic state to either $B^1\Sigma_u^+$ (Lyman band absorption) or $C^1\Pi_u$ (Werner band absorption), is usually followed by radiative decay back to the $X^1\Sigma_g^+$ electronic state. However, it is possible that this process leaves the H₂ molecule in an unbound vibrational state, resulting in its dissociation into two H atoms (a table of probabilities can be found in e.g. Dalgarno & Stephens 1970). Of course, this relies on the existence of UV radiation in the Lyman and Werner bands, which have minimum energies of 11.2 and 12.3 eV respectively. During the postrecombination era, these energies are 2–3 orders of magnitude larger than $kT_{\text{CMB}} \sim 0.2$ eV, and so the photodissociation of H₂ plays a negligible role in determining the pregalactic H₂ abundance. The presence of the spectral distortion does not change this situation since the distortion extends only up to 10.2 eV (the H I Ly α energy). It is only after the first astrophysical sources turn on that intergalactic H₂ can be destroyed.

The cosmological production of H₂ can be followed by keeping track of the abundances of the relevant species: H, He, H⁺, e⁻, H⁻, H₂⁺, HeH⁺, and H₂. The evolution of H, He, H⁺, and e⁻ has been investigated in the context of the cosmic recombination, and is essentially unaffected by the rates of the catalytic reactions Eqs. (1–5) due to the small amount of H₂ produced. We therefore use the recombination code RECFAST (Seager et al. 1999, 2000) to compute the abundances of H, H⁺, and e⁻. The rate equation for H₂ is

$$\frac{dx[\text{H}_2]}{dt} = S_- + S_+, \quad (9)$$

where S_- and S_+ are the formation rates via the H⁻ and combined H₂⁺/HeH⁺ mechanisms, respectively (note that the latter two cannot truly be separated since Eq. 8 couples them). In the next several sections, we compute the H₂ production and photodissociation rates. Section 3 treats the computation of S_- (the H⁻) mechanisms. Section 4 treats the computation of S_+ including only the H₂⁺ mechanism for simplicity. In Section 5 we introduce HeH⁺ into the computation of S_+ .

3 THE H⁻ MECHANISM

The rate for the H⁻ mechanism depends on the population of H⁻ as a function of time. The relevant rate equation is

$$\begin{aligned} \frac{dx[\text{H}^-]}{dt} &= k_1 x_e x_{\text{HI}} n - k_{-1} x[\text{H}^-] - k_2 x[\text{H}^-] x_{\text{HI}} n \\ &\quad - k_3 x[\text{H}^-] x[\text{H}^+] n, \end{aligned} \quad (10)$$

where k_1 is the rate for Eq. (1), k_{-1} is the rate for the reverse reaction, k_2 is the rate for Eq. (2), and k_3 is the rate for Eq. (3). The forward rates are given by the fits in Stancil et al. (1998):

$$\begin{aligned} k_1(T_m) &= 3 \times 10^{-16} \left(\frac{T_m}{300}\right)^{0.95} e^{-T_m/9320} \text{ cm}^3 \text{ s}^{-1}, \\ k_2(T_m) &= 1.5 \times 10^{-9} \left(\frac{T_m}{300}\right)^{-0.1} \text{ cm}^3 \text{ s}^{-1}, \text{ and} \end{aligned}$$

$$k_3(T_m) = 4 \times 10^{-8} \left(\frac{T_m}{300}\right)^{-0.5} \text{ cm}^3 \text{ s}^{-1}, \quad (11)$$

where the matter temperature, T_m , is in Kelvin. (The stimulated radiative attachment can be neglected in comparison with the spontaneous rate because the energy of the emitted photon is always at least the H⁻ binding energy, or > 0.754 eV; this is much greater than $k_B T_{\text{CMB}}$ in the redshift range of interest.) There is some uncertainty in the associative detachment rate k_2 and the mutual neutralization rate k_3 , which we will discuss in Section 6. The ratio of H⁻ destruction rate to the Hubble rate is always at least $k_2 n/H \approx 3500[(1+z)/10]^{1.3} \gg 1$, so we may treat $x[\text{H}^-]$ by the steady-state approximation,

$$x[\text{H}^-] = \frac{k_1 x_e x_{\text{HI}} n}{k_2 x_{\text{HI}} n + k_{-1} + k_3 x[\text{H}^+] n}. \quad (12)$$

The production rate for H₂ via H⁻ is then,

$$S_- = \frac{k_1 k_2 x_e x_{\text{HI}}^2 n^2}{k_2 x_{\text{HI}} n + k_{-1} + k_3 x[\text{H}^+] n}. \quad (13)$$

The photodetachment rate k_{-1} depends on the details of the radiation field and can be broken into thermal (blackbody CMB) and nonthermal (spectral distortion) parts:

$$k_{-1} = k_{-1}^{(\text{th})}(T_{\text{CMB}}) + k_{-1}^{(\text{nt})}. \quad (14)$$

The rate from the thermal photons can be computed via the principle of detailed balance,

$$\begin{aligned} k_{-1}^{(\text{th})}(T_{\text{CMB}}) &= 4 \left(\frac{m_e k_B T_{\text{CMB}}}{2\pi\hbar^2}\right)^{3/2} e^{-B(\text{H}^-)/k_B T_{\text{CMB}}} \\ &\quad \times k_1(T_{\text{CMB}}), \end{aligned} \quad (15)$$

where the factor of 4 comes from the spin degeneracy (1 for H⁻, 2 each for H and e⁻), and $B(\text{H}^-) = 0.754$ eV is the photodetachment threshold energy. Note that T_{CMB} is used here instead of T_m since photodetachment depends only on the properties of the radiation field.

In the standard calculation the thermal rates are used, i.e. $k_{-1} = k_{-1}^{(\text{th})}$. The nonthermal contribution to the photodetachment rate is

$$k_{-1}^{(\text{nt})} = nc \int_{B(\text{H}^-)/h}^{\infty} r(\nu) \sigma_{-1}(\nu) \frac{d\nu}{\nu}, \quad (16)$$

where $r(\nu)$ is the number of distortion photons per H atom per logarithmic range in frequency, and $\sigma_{-1}(\nu)$ is the photodetachment cross section, for which we use the fit by Tegmark et al. (1997),

$$\sigma = 3.486 \times 10^{-16} \frac{(x-1)^{3/2}}{x^{3.11}}, \quad (17)$$

where $x = h\nu/B(\text{H}^-)$. The variable $r(\nu)$ is related to the phase space density $f(\nu)$ of photons by

$$f(\nu) = \frac{1}{e^{h\nu/k_B T_{\text{CMB}}} - 1} + \frac{nc^3}{8\pi\nu^3} r(\nu), \quad (18)$$

where the first term denotes the thermal CMB contribution, and the latter term is the spectral distortion. The spectral distortion dominates at high frequencies, $h\nu/k_B T_{\text{CMB}} > 30$.

The spectral distortion $r(\nu)$ is calculated as in Switzer & Hirata (2005): the H I 2s \rightarrow 1s two-photon decay and Lyman- α resonance escape rates were obtained from RECFAST and integrated as described in Section II

of Switzer & Hirata (2005). We note that a recent computation by Wong et al. (2006) find an additional distortion due to He I $2^1S_0 \rightarrow 1^1S_0$ two-photon decays and escape from the $2^1P_1^o \rightarrow 1^1S_0$ resonance. As can be seen from Fig. 3 of Wong et al. (2006), the He I distortion contributes significantly to the photon spectrum at short wavelengths $\lambda < 140(1+z)^{-1} \mu\text{m}$, and could be a significant contribution to H^- or H_2^+ destruction rates. However, these photons are in the H I Lyman continuum ($\lambda < 912 \text{ \AA}$) at $z \sim 1500$, when the universe is already optically thick ($\tau \sim 10^7$) due to H I photoionization. Thus we do not expect the high-energy spectral distortion from He I recombination to survive and have not included it in our analysis.

4 THE H_2^+ MECHANISM

The H_2^+ mechanism is more complicated to analyze than the H^- mechanism because unlike H^- , the H_2^+ ion has many bound states. One must therefore determine the populations of each H_2^+ level, taking into account the radiative association rates to each level, the radiative and collisional rates for changing the rotational and vibrational quantum numbers, and the destruction rates by photodissociation and charge transfer. We start with an overview of the physics of the H_2^+ ion, and describe the full reaction network that describes the ion. Finally, we show how the relevant physics can be captured by a ‘‘two-level’’ approximation; this provides a computationally simpler approach to the H_2^+ mechanism.

The H_2^+ ion is diatomic, and can be described by specifying the electronic state, a rotational quantum number N describing the total orbital angular momentum, and a vibrational quantum number v equal to the number of radial nodes. The electronic states of interest to us are the ground state $1s\sigma_g$ ($X^2\Sigma_g^+$) and the first excited state $2p\sigma_u$ ($A^2\Sigma_u^+$); higher states are not accessible at the temperatures under consideration. We ignore the spin-orbit coupling and hyperfine structure since their energy splittings are small compared to $k_B T_m$ or $k_B T_{CMB}$. Thus the degeneracy of a given rotational-vibrational level is $g_{vN} = 2(2N+1)g'_{\text{nuc}}$, where the 2 comes from the electron spin. The nuclear degeneracy is forced by proton wave function antisymmetry considerations to be $g'_{\text{nuc}} = 1/4$ for spatially symmetric states and $g'_{\text{nuc}} = 3/4$ for spatially antisymmetric states. Almost all of the bound states of H_2^+ are in the $1s\sigma_g$ ground electronic state, which has an attractive potential with a minimum energy of $E_{\text{min}} = -2.79 \text{ eV}$ at an internuclear separation $R = 1.06 \text{ \AA}$. The next-lowest electronic state $2p\sigma_u$ is repulsive (except for a weak attractive region at large distance due to the polarizability of H).

The radiative association reaction (Eq. 4) begins with an H(1s) atom and H^+ ion approaching each other. This initial electronic state is a superposition of the $1s\sigma_g$ and $2p\sigma_u$ states of H_2^+ . Because of dipole selection rules, the system can only produce an $\text{H}_2^+(1s\sigma_g)$ ion from the $2p\sigma_u$ initial electronic state. This state is repulsive, so at low initial energies the wave function is confined to large internuclear separation R . Wave function overlap considerations then imply that radiative association to highly excited $\text{H}_2^+(1s\sigma_g)$ states is preferred, since these states have significant wave functions at large R . Conversely, direct radiative association to the ground state ($N = v = 0$) is suppressed. This state of

H_2^+ can be populated by radiative transitions from excited states, but the inversion symmetry of the H_2^+ ion implies that these must be electric quadrupole transitions, hence they are slow, compared to destruction of H_2^+ . This circumstance results in level populations of H_2^+ that are very far from LTE. The non-LTE distribution, with higher-energy levels overpopulated relative to the Boltzmann distribution, results in photodissociation cross sections that are significantly higher than the commonly used LTE cross sections of Argyros (1974) and Stancil (1994).

4.1 Rate equations

The level populations of H_2^+ are determined by the solution of a network of production, destruction, and level-changing reactions. Schematically, one may write

$$\frac{dx_i}{dt} = s_i + \sum_j R_{ij}x_j - \sum_j R_{ji}x_i - \gamma_i x_i, \quad (19)$$

where s_i is the rate of production of the i th level of H_2^+ (in units of ions per H nucleus per second), R_{ij} is the rate for transitions from the i th level to the j th level, and γ_i is the rate for destruction of H_2^+ ions in the i th level. Note that the level index i encodes both the vibrational and rotational quantum numbers: $i = (v, N)$. We track all 423 bound levels of the ground electronic state, which have quantum numbers ranging up to $v = 19$ and $N = 35$.

The source function of H_2^+ comes from the radiative association reaction (Eq. 4) and its rate is given by

$$s_i = \alpha_i x[\text{H}^+] x_{\text{HIn}}. \quad (20)$$

The level-changing rates include both radiative and collisional rates, $R_{ij} = R_{ij}^{(\text{rad})} + R_{ij}^{(\text{col})}$. The radiative rates are given by the standard expression

$$R_{ij}^{(\text{rad})} = \begin{cases} A_{ij}[1 + f(\nu_{ij})] & E(i) < E(j) \\ A_{ji}f(\nu_{ji})g_i/g_j & E(j) > E(i) \end{cases}, \quad (21)$$

where A_{ij} is the Einstein coefficient. In principle there is also a collisional term $R_{ij}^{(\text{col})}$, which could accelerate H_2 production by de-activating H_2^+ ions into lower energy levels. These lower-energy ions would survive longer since they suffer less photodissociation, and hence have a higher probability of undergoing charge transfer to produce H_2 . However, it is not possible to produce more H_2 molecules by this mechanism than there are de-activating H_2^+ -H collisions. We will show in Section 6 that even if we assume the Langevin rate for charge transfer $\text{H}_2^+(\text{H}, \text{H}^+)\text{H}_2$, we find that only ~ 0.005 per cent of the H_2 is produced via the H_2^+ mechanism. Thus our conclusions about the final H_2 abundance are unaffected except in the highly unlikely circumstance that the de-activation rate coefficient is several orders of magnitude larger than the Langevin rate.

The destruction of H_2^+ proceeds by photodissociation (reverse of Eq. 4), charge transfer (Eq. 5), or dissociative recombination (Eq. 6), at a rate γ_i ,

$$\gamma_i = \beta_i + k_i^{(\text{ct})} x_{\text{HIn}} + k_i^{(\text{dr})} x_e n. \quad (22)$$

The radiative association and dissociation rates α_i and β_i , and the quadrupole Einstein coefficients A_{ij} , are computed in Appendix A. We examine the charge transfer (Section

4.2) and dissociative recombination (Section 4.3) reactions in the following sections.

As described in Section 4.3, we neglect $k_i^{(\text{dr})}$ since it is small during the regime where the H₂⁺ mechanism is most active; but if it were included, its only possible effect would be to further reduce the already negligible H₂ yield from this mechanism.

Eq. (19) possesses a steady-state solution

$$\mathbf{x} = \mathbf{T}^{-1} \mathbf{s}, \quad (23)$$

where we have written the level populations as a vector and the matrix \mathbf{T} is given by

$$T_{ij} = -R_{ij} + \delta_{ij} \left(\gamma_i + \sum_k R_{ki} \right), \quad (24)$$

which is valid if all the eigenvalues of \mathbf{T} are large (fast) compared to the Hubble time. The H₂ production rate via the H₂⁺ mechanism is then

$$S_+ = n_{\text{HI}} \sum_i k_i^{(\text{ct})} x_i. \quad (25)$$

4.2 Charge transfer

In order to complete our analysis, we need the rate of the charge transfer reaction (Eq. 5) as a function of the matter temperature for each level of the initial-state H₂⁺ ion. Unfortunately, there are no published computations of the state-resolved rates (Lepp et al. 2002). Most pregalactic chemistry networks have used the value

$$k^{(\text{ct})} = (6.4 \pm 1.2) \times 10^{-10} \text{ cm}^3 \text{ s}^{-1} \quad (26)$$

measured by Karpas et al. (1979) in an ion cyclotron resonance device; however the dependence on the temperature and initial state was not determined. Krstić (2002) has computed cross sections for Eq. (5) resolved into individual vibrational levels. but was motivated by studies of controlled fusion plasmas and so only extends down to thermal energies ($\frac{3}{2}k_B T_m = 0.1 \text{ eV}$ at $z = 300$) for some of the levels.

Given that the rate for Eq. (5) has not been measured or calculated accurately for all relevant levels, we have run our calculation for three different cases. In case (A), we use the Karpas et al. (1979) rate coefficient (Eq. 26) for all levels; in case (B) we have used the Langevin rate coefficient, $k^{(\text{ct})} = 2.38 \times 10^{-9} \text{ cm}^3 \text{ s}^{-1}$; and in case (C) we have linearly interpolated the values of σv_{rel} from Krstić (2002) and obtained a reaction rate by integrating over a Maxwellian energy distribution,

$$k_i^{(\text{ct})} = \frac{2}{\sqrt{\pi} (k_B T_m)^{3/2}} \int_0^\infty E^{1/2} e^{-E/k_B T_m} \sigma v_{\text{rel}} dE, \quad (27)$$

where E is the kinetic energy of the H+H₂⁺ system in the centre-of-mass frame and v_{rel} is the initial relative velocity of H and H₂⁺. For energies less than the lowest tabulated value (0.17 eV in the case of the $v = 0$ state) we have assumed σv_{rel} to be constant. This probably overestimates the reaction rate since for most levels σv_{rel} is an increasing function of collision energy.

4.3 Dissociative recombination

It is possible for dissociative recombination (Eq. 6) to reduce the production of H₂. In general dissociative recombination can be important if it contributes significantly in Eq. (22), i.e. if

$$k_i^{(\text{dr})} \gtrsim \frac{x_{\text{HI}}}{x_e} k_i^{(\text{ct})} \approx x_e^{-1} k_i^{(\text{ct})}. \quad (28)$$

Of the various models we consider, the lowest value of $k_i^{(\text{ct})}$ occurs for model A, with $k_i^{(\text{ct})} = 6.4 \times 10^{-10} \text{ cm}^3 \text{ s}^{-1}$. At $z < 600$ where the H₂⁺ mechanism is most active, we have $x_e < 10^{-3}$ so in order for dissociative recombination to be important, $k_i^{(\text{dr})}$ would have to be $\gtrsim 6 \times 10^{-7} \text{ cm}^3 \text{ s}^{-1}$. The tabulated rate coefficients for the first 78 levels of H₂⁺ are less than this for $20 \leq T_m \leq 5000 \text{ K}$ (Schneider et al. 1994; the maximum value in the table is $3.1 \times 10^{-7} \text{ cm}^3 \text{ s}^{-1}$ at $T_m = 20 \text{ K}$, and $1.3 \times 10^{-7} \text{ cm}^3 \text{ s}^{-1}$ for $T_m \geq 100 \text{ K}$); we therefore neglect dissociative recombination. This may not be a valid approximation at $z > 600$ where $x_e > 10^{-3}$, or for the highest excited levels of H₂⁺ (for which no published rates are available). If dissociative recombination is important in these circumstances, the effect would be to decrease the H₂ abundance at $z > 300$. There would not be a significant effect at lower redshifts, because at $z < 300$ the production of H₂ is dominated by the H⁻ and HeH⁺ mechanisms; H⁻ is unaffected by dissociative recombination, and HeH⁺ produces H₂⁺ in one of the low-lying states for which we have already concluded that dissociative recombination is irrelevant.

4.4 A “two-level” approximation

Although the above discussion completely specifies the solution for the H₂⁺ channel, it is useful to consider an approximate “two-level” solution. This serves both as a check of the more involved numerical calculations above, as well as highlighting the essential physics behind this channel.

We start by describing the H₂⁺ channel by the following two level decomposition

- H₂⁺ forms in an excited state H₂⁺⁽ⁱ⁾, at a rate α_i ,



- The excited ion is then either photodissociated at rate β_i ,



or transitions to a LTE distribution via a quadrupole transition at rate \mathcal{R}_i ,



Note that although this is a two level description, we still consider all energy levels i ; they are now however decoupled from each other.

Given Eqs. 29 to 31, we can write out the differential equations describing the time evolution of the abundances of these species. Furthermore, as before, Eqs. 30 and 31 occur significantly faster than the Hubble time, and so, we use the steady-state approximation to eliminate any explicit mention of the H₂⁺⁽ⁱ⁾ abundance. This yields the following equation for the H₂⁺ abundance,

Table 1. The suppressed association rate as a function of redshift, Eq. 34).

z	$\log_{10} \alpha' \text{ (cm}^3 \text{ s}^{-1}\text{)}$	z	$\log_{10} \alpha' \text{ (cm}^3 \text{ s}^{-1}\text{)}$
50	-21.8824	300	-22.1023
100	-22.1048	350	-22.2281
150	-21.9867	400	-22.3786
200	-21.9676	450	-22.5421
250	-22.0103	500	-22.7089

$$\frac{dx[\text{H}_2^+]}{dt} = \left(\sum_i \frac{\alpha_i \mathcal{R}_i}{\mathcal{R}_i + \beta_i} \right) n x_{\text{HI}} x[\text{H}^+] - \beta x[\text{H}_2^+], \quad (32)$$

where β is now the LTE photodissociation rate (determined by averaging β_i as calculated in Appendix A over the Boltzmann distribution of levels at the CMB temperature). Finally, there remains the issue of what to assume for \mathcal{R}_i ; for simplicity, we assume that \mathcal{R}_i is the total transition probability to lower levels,

$$\mathcal{R}_i = \sum_{E(j) < E(i)} A_{ji} [1 + f(\nu_{ji})]. \quad (33)$$

Note that Eq. 32 now resembles the standard H_2^+ calculation with a suppressed radiative association rate,

$$\alpha' = \sum_i \frac{\alpha_i \mathcal{R}_i}{\mathcal{R}_i + \beta_i}. \quad (34)$$

Note that the error in this approximation could go either direction. This is because, although our nascent H_2^+ ion is likely to be produced in a highly excited state, we do not really know without the full multi-level calculation whether *after* it emits its first photon the resulting distribution is “more excited” or “less excited” than Boltzmann. We defer a comparison of this approximation with the full calculation until Section 6, and conclude by tabulating the suppressed association rate as a function of redshift (Table 1).

5 THE HeH^+ MECHANISM

The HeH^+ mechanism is really an additional set of reactions that couple to Eqs. (4–6). Therefore the most straightforward way to include it is to add HeH^+ as an additional “level” in the network of Section 4.1. Due to its large dipole moment, HeH^+ has very short-lived excited levels (lifetime $\sim 10^{-3}$ s; Roberge & Dalgarno 1982). These lifetimes are short compared to the photodissociation time from these levels or the time between collisions ($\sim 10^8$ s at $z = 300$), so the distribution of level populations is determined entirely by the radiation field. In the absence of a spectral distortion, then, it would be permissible to assume that the level populations of HeH^+ are in LTE at the CMB temperature T_{CMB} .

In reality there is a spectral distortion, however its effect on HeH^+ is negligible. The distortion photons that would affect HeH^+ are those at $E > 1.6[(1+z)/250]$ eV, where the distortion is significant compared to the thermal CMB radiation; there is roughly 1 distortion photon in this energy range per H atom. Since the rate coefficient for H_2^+ formation from HeH^+ via Eq. (8) is $9.1 \times 10^{-10} \text{ cm}^3 \text{ s}^{-1}$ (Karpas et al.

1979), photodissociation of HeH^+ by distortion photons can be significant if the photodissociation cross section averaged over the HeH^+ level and distortion photon energy distributions is $\sigma c \sim 9.1 \times 10^{-10} \text{ cm}^3 \text{ s}^{-1}$. The cross section for photodissociation from the $v = 0$ level of HeH^+ is always $\sigma c < 1.5 \times 10^{-12} \text{ cm}^3 \text{ s}^{-1}$ (Roberge & Dalgarno 1982). The cross section from the higher excited states $v = 7$ and $v = 8$ is $\sigma c \sim 3 \times 10^{-9} \text{ cm}^3 \text{ s}^{-1}$ near threshold (Saha et al. 1978) and could, in principle, be important, except that the fraction of HeH^+ in these states is $\ll 1$ (they lie 1.56 and 1.62 eV above the ground state, as compared with $k_B T_{\text{CMB}} = 0.07$ eV at $z = 300$). Hence the HeH^+ levels are in LTE at the CMB temperature T_{CMB} and HeH^+ can be followed as an “effective 1-level” molecular ion.

It is straightforward to write down the additional terms in Eqs. (20–22) to take into account the HeH^+ contribution. The additional source is due to radiative attachment,

$$s_{\text{HeH}^+} = \alpha_{\text{HeH}^+} x[\text{He}] x_{\text{HI}} n, \quad (35)$$

where α_{HeH^+} is the radiative attachment rate coefficient. The destruction term is simply the photodissociation rate,

$$\gamma_{\text{HeH}^+} = \beta_{\text{HeH}^+}. \quad (36)$$

Finally the transition matrix \mathbf{R} picks up two additional terms due to Eq. (8). One is the forward reaction term

$$R_{i, \text{HeH}^+} = k_8 f_i^{(8)} x_{\text{HI}} n, \quad (37)$$

where k_8 is the rate coefficient for Eq. (8) and $f_i^{(8)}$ is the branching fraction to the i th level of H_2^+ . The other is the reverse reaction, which can be obtained by the principle of detailed balance,

$$R_{\text{HeH}^+, i} = R_{i, \text{HeH}^+} e^{[E(i) + D_0(\text{HeH}^+)]/k_B T_m} \times \frac{2Q(\text{HeH}^+, T_m)}{g_i} \left(\frac{\mu_{\text{HeH}^+ + \text{H}}}{\mu_{\text{He} + \text{H}_2^+}} \right)^{3/2}. \quad (38)$$

The ratio of reduced masses is $\mu_{\text{HeH}^+ + \text{H}}/\mu_{\text{He} + \text{H}_2^+} \approx 5/8$, and the partition function $Q(\text{HeH}^+)$ is obtained at the matter temperature T_m from Engel et al. (2005). The binding energy is $D_0(\text{HeH}^+) = 1.84412$ eV (Zygelman et al. 1998). The factor of 2 comes from the ground state degeneracy of H (He has degeneracy 1). The remaining additional term in the transition matrix is $R_{\text{HeH}^+, \text{HeH}^+} = 0$.

To compute the H_2 production, one must also know α_{HeH^+} , β_{HeH^+} , $k_{(8)}$, and $f_i^{(8)}$. For α_{HeH^+} , we have used the fit by Galli & Palla (1998) to the results of Roberge & Dalgarno (1982). This rate can in principle be increased by stimulated radiative association. However Zygelman et al. (1998) found that this increases the HeH^+ abundance by < 20 per cent in the redshift range of interest, and since our analysis does not change the formation and/or destruction mechanisms a similar result would apply to our case. We have thus not included a correction for stimulated radiative association (we will see that the HeH^+ mechanism is not a major source of primordial H_2 , so a correction of this magnitude in HeH^+ abundance translates into a much smaller correction to the net H_2 production). For β_{HeH^+} , we have used the principle of detailed balance,

$$\beta_{\text{HeH}^+} = \frac{1}{Q(\text{HeH}^+, T_{\text{CMB}})} \left(\frac{\mu k_B T_{\text{CMB}}}{2\pi \hbar^2} \right)^{3/2}$$

$$\times e^{-D_0(\text{HeH}^+)/k_B T_{\text{CMB}}} \alpha_{\text{HeH}^+}(T_{\text{CMB}}); \quad (39)$$

here μ is the reduced mass of He and H⁺. The rate coefficient $k_{(8)}$ has been measured by Karpas et al. (1979) to be $9.1 \times 10^{-10} \text{ cm}^3 \text{ s}^{-1}$. For the $f_i^{(8)}$, which control the distribution of rotation-vibration levels in the final state of Eq. (8), there do not appear to be any published measurements or calculations. We have thus considered two cases: one in which Eq. (8) populates all energetically available levels with their statistical ratios, and one in which the reaction always leaves H₂⁺ in the ground state of either para-H₂⁺ ($v = 0, N = 0$; probability 1/4) or ortho-H₂⁺ ($v = 0, N = 1$; probability 3/4). While the two cases lead to different level populations of H₂⁺, the total abundances $x[\text{H}_2^+](z)$ and $x[\text{H}_2](z)$ are unaffected. This is because, for any of the H₂⁺ levels accessible to Eq. (8) at thermal energies, the most probable fate of the H₂⁺ ion is to radiate away its vibrational energy on a timescale of order 10^7 s, and then to undergo charge exchange to produce H₂ on a timescale of order 10^9 s. Thus the information about the initial (v, N) distribution of the H₂⁺ is erased. Photodissociation from the low- v levels of H₂⁺ is strongly suppressed due to lack of wave function overlap, and electric quadrupole excitation to high- v levels followed by photodissociation is slower than charge transfer; thus photodissociation is not effective at depleting the H₂⁺ produced by Eq. (8). The case where all energetically available levels are populated with their statistical ratios will be used in the rest of this paper.

6 RESULTS: H₂ ABUNDANCE

We now present the results of integrating the production rate of H₂ from the three major mechanisms. The total production of H₂ is obtained by the integral

$$x[\text{H}_2] = \int (S_- + S_+) dt, \quad (40)$$

which is shown in Fig. 1. The production rate per Hubble time $(S_- + S_+)/H$ is shown in Fig. 2. The abundances of the intermediates H⁻, H₂⁺, and HeH⁺, obtained from Eqs. (12, 23), are shown in Fig. 3.

6.1 H⁻

In our calculation, the final H₂ abundance is determined essentially entirely by the H⁻ reaction sequence. In accordance with previous calculations, at high redshift ($z > 140$) the H⁻ ion is formed mainly through radiative attachment, and destroyed mainly through photodetachment by thermal CMB photons. Note that this is not quite a Saha-type equilibrium because of the different matter and radiation temperatures. At $z \approx 127$, the spectral distortion begins to dominate the photon spectrum at energies of ~ 1 eV, where the H⁻ photodetachment cross section peaks. Below this redshift, H⁻ is still produced mainly by radiative attachment, but the destruction mechanism is photodetachment from distortion photons. This situation remains until $z \approx 67$, when most of the spectral distortion has redshifted to below the H⁻ photodetachment threshold. At this time, the competing photodetachment and associative detachment (Eq. 2) rates are

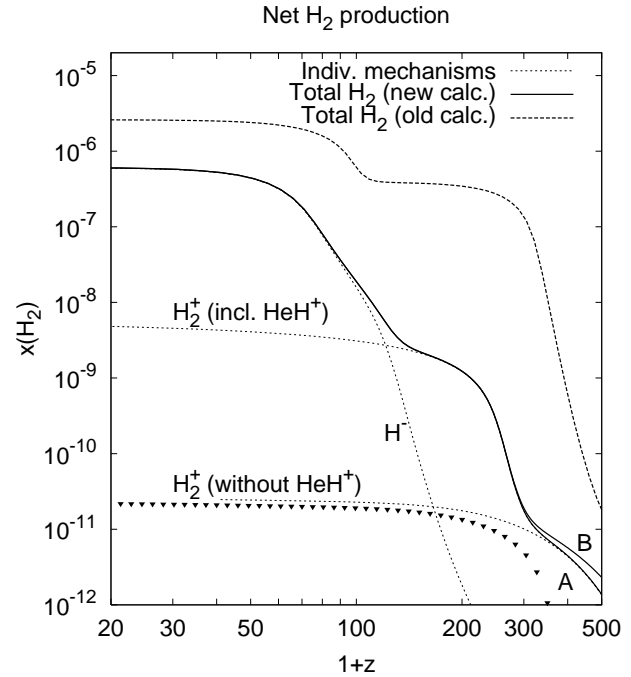


Figure 1. The total abundance of H₂ as a function of redshift. The thick solid lines shows the new calculation of H₂ abundance for models A and B (C is indistinguishable from B on the scale of the plot). The thick long-dashed line shows the old calculation, which overestimated $x[\text{H}_2]$. The thin short-dashed lines show the individual production mechanisms: H⁻, H₂⁺/HeH⁺, and H₂⁺ (without HeH⁺). The triangles indicate the results for H₂⁺ only from the simplified model of Section 4.4.

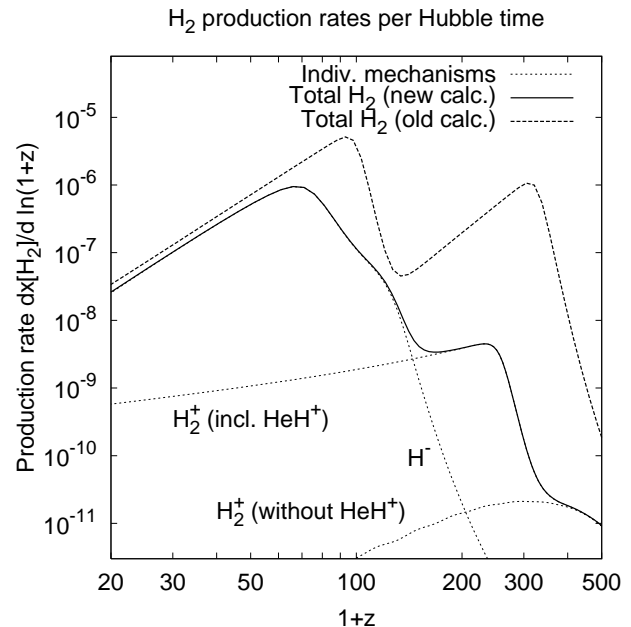


Figure 2. The production rate of H₂ via the H⁻, H₂⁺, and HeH⁺ mechanisms, in units of H₂ molecules per hydrogen nucleus per Hubble time. The thick solid line shows the new calculation of H₂ rate for models A, while the thick long-dashed line shows the old calculation. The thin short-dashed lines break down the H₂ production into the individual mechanisms.

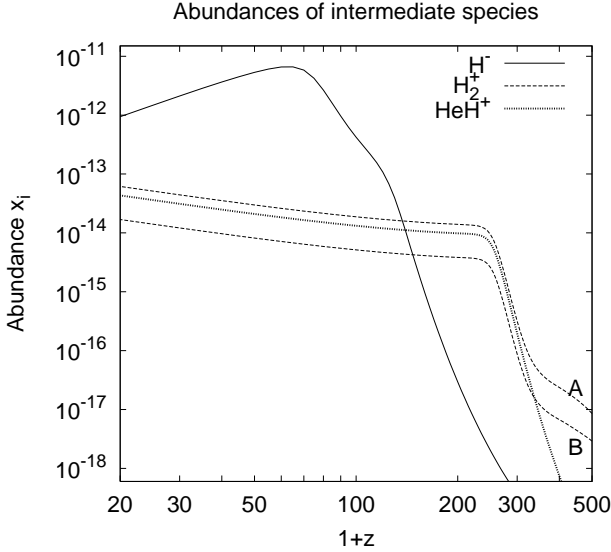


Figure 3. The abundances of the intermediates H^- , H_2^+ , and HeH^+ . The H_2^+ curve is shown for both models A and B. Note that $x[\text{H}^-]$ peaks at $z \approx 62$ when H_2 production is also maximized.

similar ($\sim 10^{-10} \text{ s}^{-1}$). This is also the era of peak production of H_2 : at higher redshifts the H^- ions are destroyed before they can react with H to produce H_2 , while at lower redshifts less H^- is produced due to the lower density of the universe and the decrease in reaction rate at low T_m . Ultimately we find that the total amount of H_2 produced via the H^- mechanism, $\int S_- dt$, is only 6×10^{-7} instead of 2.2×10^{-6} as found in the standard calculation.

As noted in Section 3, there is some uncertainty in the rate for associative detachment, Eq. (2). Glover et al. (2006) argued that the rate coefficient k_2 could plausibly be varied between 6.5×10^{-10} and $5 \times 10^{-9} \text{ cm}^3 \text{ s}^{-1}$. We have re-run our analysis using these values and find that the final H_2 abundance varies from $x[\text{H}_2] = 4.1 \times 10^{-7}$ for the lowest value of k_2 to 9.4×10^{-7} for the highest value. Thus our fiducial estimate of 6×10^{-7} should be considered uncertain by a factor of ~ 1.5 in either direction.

There is also a large uncertainty in the mutual neutralization rate, with some results (e.g. the experimental work of Moseley et al. 1970) being up to an order of magnitude higher than the fits used here. Using the higher mutual neutralization rate determined by the fit of Moseley et al. (1970), we find that the final H_2 abundance decreases from 6.0×10^{-7} to 5.7×10^{-7} . Thus the uncertainty in the mutual neutralization rate does not have a significant effect on the final H_2 abundance.

6.2 H_2^+ and HeH^+

We find that the reactions involving positive ions (Eqs. 4–8) do not contribute significantly to the final H_2 abundance. Nevertheless these reactions operate at earlier times than H^- due to the higher binding energy of HeH^+ and H_2^+ compared to H^- , and so they dominate the H_2 production at $z > 144$. The total amount of H_2 produced by these reactions

is $\int S_+ dt = 5 \times 10^{-9}$, with almost all of this contributed by HeH^+ .

Our computed HeH^+ abundance (see Fig. 3) are very similar to those obtained in previous works (Galli & Palla 1998; Stancil et al. 1998). In contrast, we find much lower H_2^+ ion abundances (and H_2 production rates via H_2^+) than in the standard calculation. This is a consequence of the non-Boltzmann level populations in H_2^+ . An example of these level populations for model A at $z = 300$ is shown in Fig. 4. (Results are qualitatively similar for model B, with the main quantitative difference being that the lowest-energy states are less populated.) As shown in the figure, the highest-lying levels are nearly in Boltzmann equilibrium since the reaction



is fast compared with the electric quadrupole transitions in H_2^+ . (The slight deviation from Boltzmann equilibrium among the high-lying levels in the figure is due to the difference between matter and radiation temperatures.) The populations of the lower-lying levels are determined by a combination of quadrupole radiative cascade rates, sourcing by HeH^+ through Eq. (8), and (at the lowest energies) some quadrupole excitation by the CMB. Note that even in the ground vibrational state ($v = 0$), the rotational levels of H_2^+ never come to thermal equilibrium with the CMB because the radiative rates (which may be as long as $\sim 10^{10} \text{ s}$) are slower than the timescale for charge transfer (about $3 \times 10^8 \text{ s}$ for model A at $z = 300$).

The overall production of H_2 via the $\text{HeH}^+/\text{H}_2^+$ mechanisms is found to be $x[\text{H}_2] = 4.8 \times 10^{-9}$ at $z = 20$. Of this, only a small fraction ($x[\text{H}_2] = 2.6 \times 10^{-11}$) is formed if we artificially turn off HeH^+ . (These numbers are for model A, models B and C give numbers that are < 10 per cent higher.) The direct production of H_2^+ via Eq. (4) only contributes significantly at $z > 300$ where it is possible to directly produce tightly bound states by radiative association.

The two-level model of Section 4.4 does quite well at reproducing the final H_2 abundance due to H_2^+ (it yields 2.2×10^{-11} versus 2.6×10^{-11} for the full multi-level calculation). It is not quite so good at reproducing the redshift history: at very high redshifts where H_2^+ can be excited out of the ground state and photodissociated, it underestimates H_2 production because the photodissociation rate of the H_2^+ ion after it has reached a low-lying level is actually less than the LTE rate.

7 HEATING

The principal reason for interest in the molecular abundances in primordial gas is the possible effect on the heating and cooling rates. Before the formation of collapsed structures, the gas is colder than the CMB and hence the effect of molecular transitions is to heat the gas; after collapse the gas is compressed and shock-heated to above the CMB temperature, at which point molecules cool the gas. The latter regime is dominated by H_2 molecules formed in the collapsed gas clouds themselves rather than primordial molecules, and hence it is not considered here. The molecular heating in the pre-collapse regime was first investigated by Puy et al. (1993), and later by Haiman et al. (1996a), Galli & Palla

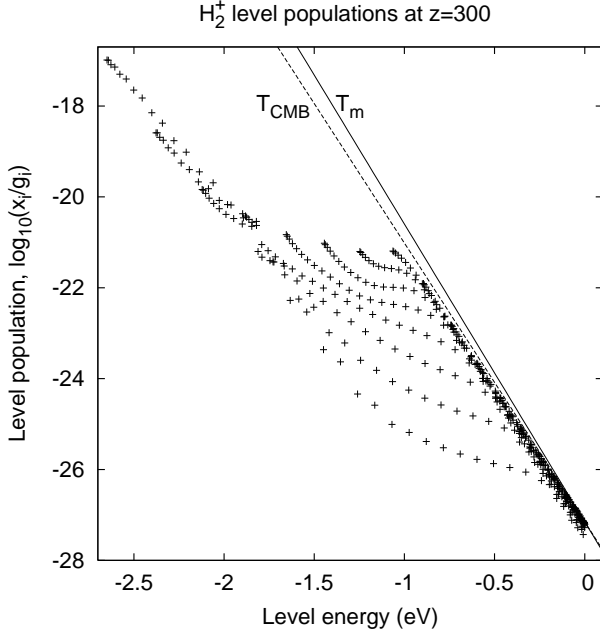


Figure 4. The level populations in H₂⁺ at $z = 300$ for model A. The horizontal axis shows the level energy with $E = 0$ defined as the dissociation limit into H+H⁺. The actual populations for each of the 423 rotational-vibrational levels are given by the crosses. The Boltzmann equilibrium populations $\propto e^{-E/k_B T}$ at the radiation and matter temperatures are shown by the straight lines. Note that the levels close to the continuum are approximately in equilibrium, but the low-lying levels are highly underpopulated relative to Boltzmann. The levels more tightly bound than $E(vN) < -1.844$ eV have higher populations because they can be formed from HeH⁺ via Eq. (8). At this redshift the radiation and matter temperatures are $k_B T_{CMB} = 0.0708$ eV and $k_B T_m = 0.0662$ eV, respectively.

(1998), and Flower & Pineau des Forêts (2000). The purpose of this section is to revisit the heating rate, taking into account the revised molecular production rates, and including the release of heat in chemical reactions. The chemical heating was considered by Puy et al. (1993) and found to be “negligible,” but no quantitative result was given; in any case we have found large changes in some of the relevant reaction rates and it is only prudent to re-evaluate the chemical heating term.

The overall temperature balance equation is

$$\frac{dT_m}{dt} = -2HT_m + \frac{8\sigma T_{CMB}^4}{3m_e c} (T_{CMB} - T_m) + \frac{2}{3k_B x_t} (Q_{ff} + Q_{rec} + Q_{rot} + Q_c) - \frac{T_m}{x_t} \frac{dx_t}{dt}, \quad (42)$$

where the first term represents the adiabatic expansion, the second term represents Compton heating, the third term represents heating by molecular rotation and chemical reactions, and the fourth term takes account of the changing number of translational degrees of freedom among which kinetic energy is distributed (Puy et al. 1993). In this equation, σ_T is the Thomson cross section; a_{bb} is the blackbody radiation coefficient; m_e is the electron mass; x_t is the number of gas particles per H nucleus; Q_{ff} is the free-free heating rate; Q_{rec} is the net heating due to recombinations (note that this is negative); Q_{rot} is the heating by molecular rota-

tion per H nucleus per unit time; and Q_c is the heating by chemical reactions per H nucleus per unit time.

7.1 Rotational transitions

In this section we evaluate the heating in the rotational lines of H₂. It is found to be negligible, and is much smaller than the direct heating produced by the chemical reactions that generate H₂. Determining the rotational line heating requires determining first the level populations and then computing the heating rates by considering all collisional excitations and de-excitations via H and H⁺.

The H₂ molecule has two sets of levels with different nuclear spin properties, namely para-H₂ (even angular momentum J , and total nuclear spin $I = 0$) and ortho-H₂ (odd J ; $I = 1$).¹ In the high-redshift universe, the timescale for the electric quadrupole radiative transitions that connect H₂ levels with the same nuclear spin is fast compared to the timescale for collisions. For example, using the radiative rates of Turner et al. (1977) and the collisional rates described below, we find that the collisional-to-radiative transition rate ratio at $z = 250$ is 0.04 for $J = 0$; this rate is even less for higher rotational levels or lower redshifts. Therefore we may treat the H₂ molecule as an effective two-level system, tracking separately the abundances of para-H₂ and ortho-H₂. Within each set of levels (even or odd J), the populations are assumed to rapidly thermalize to the CMB temperature, $x[\text{H}_2, J] \propto g_J e^{-E_J/k_B T_{CMB}}$. Here the degeneracy is $g_J = (2J + 1)/4$ for even J or $g_J = 3(2J + 1)/4$ for odd J . The evolution equation for the fraction \mathcal{F} of the H₂ molecules in the ortho form is

$$\frac{d\mathcal{F}}{dt} = (\mathcal{F}_{\text{prod}} - \mathcal{F}) \frac{d}{dt} \ln x[\text{H}_2] + \gamma_{p \rightarrow o}(1 - \mathcal{F}) - \gamma_{o \rightarrow p} \mathcal{F}, \quad (43)$$

where $\mathcal{F}_{\text{prod}}$ is the fraction of H₂ that is produced in the ortho levels; $\gamma_{p \rightarrow o}$ is the para-to-ortho transition rate (in s⁻¹); and $\gamma_{o \rightarrow p}$ is the ortho-to-para transition rate. The transition rates are

$$\gamma_{p \rightarrow o} = n \left(x[\text{H}^+] \langle \sigma_{p \rightarrow o} v \rangle_{\text{H}_2 + \text{H}^+} + x_{\text{HI}} \langle \sigma_{p \rightarrow o} v \rangle_{\text{H}_2 + \text{H}} \right), \quad (44)$$

where the averages are taken over both thermal velocity at temperature T_m and the Boltzmann distribution of H₂ rotational levels. A similar equation holds for $\gamma_{o \rightarrow p}$. We have taken the cross sections for H₂+H⁺ from Gerlich (1990). For H₂+H, we have used the fits by Flower (1997), with the correction for reactive scattering by Le Bourlot et al. (1999). Also, since H₂ is usually produced in a highly excited rotational state when it forms from H⁻+H (Launay et al. 1991), we have assumed here that $\mathcal{F}_{\text{prod}} = 3/4$ as would be suggested by the nuclear spin degeneracy. Once the level populations are established, the heating rate is computed by assuming that an amount of energy $E_J - E_{J'}$ is added to the translational degrees of freedom of the gas for each collisional $J \rightarrow J'$ transition:

$$Q_{rot} = \sum_{J, J'} x[\text{H}_2, J] (E_J - E_{J'}) n \left(x[\text{H}^+] \langle \sigma_{J \rightarrow J'} v \rangle_{\text{H}_2 + \text{H}^+} + x_{\text{HI}} \langle \sigma_{J \rightarrow J'} v \rangle_{\text{H}_2 + \text{H}} \right). \quad (45)$$

¹ The orbital angular momentum N and the orbital plus electron spin angular momentum J are identical for the H₂ electronic ground state since the term symbol is ¹Σ_g⁺.

Our treatment of H₂ cuts off the rotational levels at $J_{\max} = 9$, the highest level for which Gerlich (1990) provides H₂+H⁺ cross sections; but we have found that at $z < 400$ there is a < 10 per cent change in the heating rate if we cut off the levels at $J_{\max} = 7$ instead.

7.2 Chemical heating

We next consider the chemical heating from each of Eqs. (1–8). The first contribution comes from the formation and destruction of H⁻, Eq. (1). The rate of loss of kinetic energy from the forward reaction is $k_1 \bar{E}(T_m) x_e x_{\text{HI}} n$, where $\bar{E}(T_m)$ is the mean energy of the incident electron participating in the reaction. This mean energy is given by multiplying the Maxwell distribution against the radiative association cross section,

$$\begin{aligned} \bar{E} &= \frac{\int_0^\infty E^2 \sigma_{ra}(E) e^{-E/k_B T_m} dE}{\int_0^\infty E \sigma_{ra}(E) e^{-E/k_B T_m} dE} \\ &= k_B T_m^2 \frac{d}{dT_m} \ln \int_0^\infty E \sigma_{ra}(E) e^{-E/k_B T_m} dE \\ &= k_B T_m^2 \frac{d}{dT_m} \ln [T_m^{3/2} k_1(T_m)] \\ &= k_B T_m \left(\frac{3}{2} + \frac{d \ln k_1}{d \ln T_m} \right), \end{aligned} \quad (46)$$

where in the last line we have re-expressed the energy integral in terms of the thermally averaged rate coefficient. By the principle of detailed balance, the average energy of the photodetached electrons from the thermal part of the reverse reaction is given by the same function, $\bar{E}(T_{\text{CMB}})$. For the electrons that are photodetached by the spectral distortion, the kinetic energy input is $h\nu - B(\text{H}^-)$. Thus the overall heating term associated with Eq. (1) is

$$\begin{aligned} Q_{c1} &= - \left(\frac{3}{2} + \frac{d \ln k_1(T_m)}{d \ln T_m} \right) k_B T_m k_1 x_e x_{\text{HI}} n \\ &\quad + x[\text{H}^-] \left\{ \left(\frac{3}{2} + \frac{d \ln k_1(T_{\text{CMB}})}{d \ln T_{\text{CMB}}} \right) k_B T_{\text{CMB}} k_{-1}^{(\text{th})} \right. \\ &\quad \left. + \int_{B(\text{H}^-)/h}^\infty r(\nu) \sigma_{-1}(\nu) [h\nu - B(\text{H}^-)] \frac{d\nu}{\nu} \right\}. \end{aligned} \quad (47)$$

The second contribution is the heating due to associative detachment, Eq. (2). As noted by Puy et al. (1993), this reaction is exothermic by 3.72 eV; however it is not correct to set the heating term from Eq. (2) equal to 3.72 eV times the reaction rate, because this energy yield is distributed among both the kinetic energy of the ejected electron (which couples to the gas temperature) and the rotational and vibrational degrees of freedom of the H₂ molecule (which are radiated away on timescales of $\sim 10^6$ s, i.e. much shorter than the collision timescale). In order to compute the heating term, one needs to know the mean excitation energy of the final-state H₂ molecule. This can be determined from the (v, J) -resolved cross sections for associative detachment of H and H⁻, which were computed by Bieniek & Dalgarno (1979) at an initial state energy of 0.0129 eV (which is roughly the initial energy of interest); this yields a mean excitation energy of 2.81 eV. By subtraction we estimate that 0.91 eV of energy is available to heat the gas. Thus we set

$$Q_{c2} = (0.91 \text{ eV}) k_2 x[\text{H}^-] x_{\text{HI}} n. \quad (48)$$

A third contribution to the heating rate is from mutual neutralization, Eq. (3). The branching fraction for this rate is small, but it is strongly exothermic (12.84 eV) and thus provides a potentially large amount of energy. The final state products are H atoms, which have no rotational or vibrational degrees of freedom. They do however have electronic degrees of freedom: it is energetically possible for the final state to be H(1s)+H(nl) for any $0 \leq l < n \leq 4$. At low energies, nearly all of the neutralizations go to $n = 3$ (Fussen & Kubach 1986), so the energy released into translational degrees of freedom is 0.76 eV. The excited H atom decays by emitting H α , Lyman, and/or 2-photon continuum radiation, none of which can heat the gas. Therefore the mutual neutralization heating term is

$$Q_{c3} = (0.76 \text{ eV}) k_3 x[\text{H}^-] x[\text{H}^+] n. \quad (49)$$

We also consider the heating and cooling from the H₂⁺ and HeH⁺ reactions. The contribution from Eq. (4) is obtained by inserting the translational energy $E = E(vN) + h\nu$ in the integrals for radiative association (Eq. A10) and photodissociation (Eq. A5). The heating from the charge transfer reaction, Eq. (5), depends on the final rotational-vibrational state of the H₂ molecule, which is not resolved in our code. We have assumed that the H₂ is produced in the ground state, which maximizes the heating from this reaction since it implies that the entire energy yield of the reaction is available to heat the gas; however Eq. (5) is not a significant source of chemical energy anyway. The radiative association and dissociation of HeH⁺ (Eq. 7) was treated using the obvious analogue of Eq. (47), without the spectral distortion since as argued earlier it is unimportant for HeH⁺. The contribution to the heating rate from all of the H₂⁺ and HeH⁺ reactions is negligible.

7.3 Results

The results are shown in Fig. 5; it is seen that the chemical heating is very small, of the order of 10^{-4} . The principal source of heating is the H⁻ sequence of reactions, which provide a peak in the heating at $z \sim 120$ from the photodetachment process, and a second peak at $z \sim 70$ due to associative detachment. There is even less heating at earlier times, and in any case heating before Compton freeze-out ($z \sim 200$) will be erased.

We find that the heating due to rotational transitions in H₂ is negligible, in qualitative agreement with the results of Flower & Pineau des Forêts (2000). The fractional heating rate peaks at $\sim 3 \times 10^{-6}$ at $z \approx 50$, shortly after the peak in H₂ production rate (there is less H₂ at earlier times, and the decreasing density and temperature suppress collisional rates at later times). The difference from some previous results (e.g. Puy et al. 1993) is due partially to our reduced H₂ abundance but also due to reduced J -changing collision cross sections. In particular, collisions with H⁺ dominate the transfer of rotational energy into translational degrees of freedom. While there remains considerable uncertainty in the potential for the H₂+H system as noted by several authors (e.g. Galli & Palla 1998; Flower & Pineau des Forêts 2000), we find that the cross sections would have to be increased by a factor of 40 to make rotational heating con-

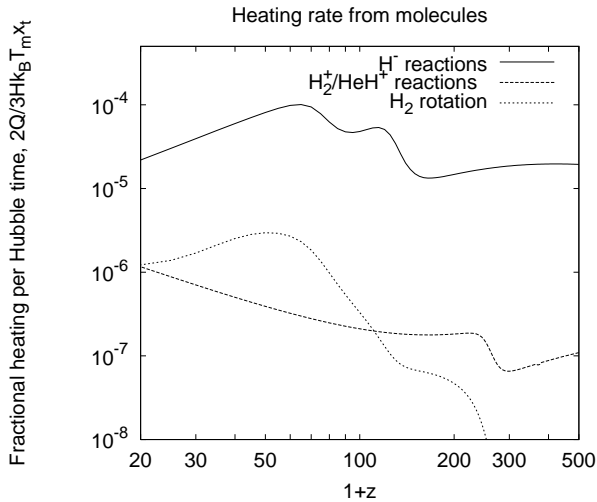


Figure 5. The heating rate due to the H⁻ and H₂⁺/HeH⁺ sequences of reactions, and the H₂ rotational transitions, for Model A. What is shown is the heating input per Hubble time, Q/H , divided by the thermal energy of the gas, $3k_B T_m x t/2$. The H⁻ reactions affect the gas temperature at the $\sim 10^{-4}$, and H₂⁺ reactions have even less influence. The H₂ rotational line heating is always small compared to the chemical reactions.

tribute at the 10^{-5} level ($2Q_r/3Hk_B T_m = 10^{-5}$), and by a factor of 500 to make it contribute at the 10^{-4} level. Thus the conclusion that rotational heating is negligible is relatively insensitive to the remaining uncertainty in H₂+H cross sections.

Chemical and H₂ rotational heating are clearly very small effects and the only proposed observational technique that could achieve the 10^{-4} level of accuracy, even in principle, is 21-cm tomography (Loeb & Zaldarriaga 2004). In practice the experimental challenges of detecting the cosmological 21-cm signal are substantial (see e.g. Bowman et al. 2006 for a recent review), and observing the pre-reionization epoch to such high accuracy should be considered a goal for the distant future. Until such data are available the chemical and rotational heating of the pregalactic gas can be safely neglected.

8 DISCUSSION

We have reconsidered the production of H₂ molecules in the pregalactic medium. In contrast to previous studies, we have included the spectral distortion in our analysis, and resolved all 423 rotational-vibrational levels of the H₂⁺ ion. We find that in the level-resolved analysis, the H₂⁺ reaction pathway is greatly suppressed because newly formed H₂⁺ ions are photodissociated before they can decay to the ground state or undergo charge transfer to become H₂ molecules. We also find that the H⁻ ion is easily destroyed by spectral distortion photons at $z > 70$, so that the production of H₂ by this pathway is suppressed relative to the standard calculation. We obtain a final H₂ abundance $x[\text{H}_2] = 6 \times 10^{-7}$ assuming standard cosmology.

Unfortunately, the primordial H₂ molecules will be very difficult to detect. The main effect of H₂ on the thermal history of the gas actually comes from the formation process

(via the H⁻ sequence, Eqs. 1, 2) rather than rotational lines; however the effect is only of the order of 10^{-4} . In principle the proposed 21-cm tomography of the pre-reionization Universe could reach the sensitivity at which primordial H₂ becomes important, since it is sensitive to the temperature of the gas and has many more than $(10^{-4})^{-2} \sim 10^8$ modes. However when assessing the prospects, it should be remembered that the high-redshift 21-cm signal has not yet been detected, and measurements at the 10^{-4} level are clearly very far in the future.

Aside from H₂, there are other molecules with rotational lines such as HD and LiH, which could conceivably have been formed in the early Universe and played a role in the thermal balance. The treatment of these trace molecules is beyond the scope of this paper, but HD in particular may warrant further study as it has been found to be a significant heating source in some past works (e.g. Puy et al. 1993). Since the main route of formation of HD is via the reaction H₂(D⁺,H⁺)HD (Galli & Palla 1998), any analysis of HD must incorporate the revised H₂ calculation presented here.

Finally, one could ask whether the H₂ suppression mechanisms discussed here – the spectral distortion and non-equilibrium populations in H₂⁺ – have a significant effect on H₂ cooling of protogalaxies. In the case of the spectral distortion, we have seen that at mean density the photodetachment of H⁻ becomes unimportant at low redshift, since H⁻ ions undergo a chemical reaction (usually associative detachment) before being destroyed by radiation. For example, the branching fraction for H⁻ at mean density to be destroyed by radiation is 0.13 at $z = 40$, 0.09 at $z = 30$, and 0.05 at $z = 20$. In overdense gas clouds at $z < 40$ the collisional reactions are faster and we conclude that the spectral distortion should be negligible. We have tried running our H₂⁺ code for overdense conditions at low redshift (e.g. $z = 20$, $\delta_b = 10^4$, $T = 10^3$ K) and find that the H₂⁺ levels are still far out of equilibrium, with the lowest levels underpopulated relative to the Boltzmann distribution (at T_{CMB}) by many orders of magnitude. However in such clouds H⁻ is likely to be a more important source of molecules than H₂⁺ (see e.g. Tegmark et al. 1997). Therefore we do not expect our changes in H₂⁺ physics to have large consequences for the cooling of the first collapsed objects in the universe.

ACKNOWLEDGMENTS

C.H. is supported in part by NSF PHY-0503584 and by a grant-in-aid from the W. M. Keck Foundation. We thank Eric Switzer and Uroš Seljak for useful discussions.

REFERENCES

- Abgrall H., Le Bourlot J., Pineau des Forêts G., Roueff E., Flower D. R., Heck L., 1992, *A&A*, 253, 525
- Argyros J. D., 1974, *J. Phys. B*, 7, 2025
- Bates D. R., 1951, *J. Chem. Phys.*, 19, 1122
- Bates D. R., Poots G., 1953, *Proc. Phys. Soc. A*, 66, 784
- Bates D. R., Ledsham K., Stewart A. L., 1953, *Phil. Trans. R. Soc. A*, 246, 215
- Bieniek R. J., Dalgarno A., 1979, *ApJ*, 228, 635

- Bowman J. D., Morales M. F., Hewitt J. N., 2006, *ApJ*, 638, 20
- Dalgarno A., Stephens T. L., 1970, *ApJ*, 160, L107
- Dunn G. H., 1968, *Phys. Rev.*, 172, 1
- Engel E. A., Doss N., Harris G. J., Tennyson J., 2005, *MNRAS*, 357, 471
- Flower D. R., 1997, *MNRAS*, 288, 627
- Flower D. R., Pineau des Forêts G., 2000, *MNRAS*, 316, 901
- Fussen D., Kubach C., 1986, *J. Phys. B*, 19, L31
- Galli D., Palla F., 1998, *A&A*, 335, 403
- Gerlich D., 1990, *J. Chem. Phys.*, 92, 2377
- Glover S. C., Savin D. W., Jappsen A. K., 2006, *ApJ*, 640, 553
- Haiman Z., Thoul A. A., Loeb A., 1996a, *ApJ*, 464, 523
- Haiman Z., Rees M. J., Loeb A., 1996b, *ApJ*, 467, 522
- Halverson N. W. et al., 2002, *ApJ*, 568, 38
- Hinshaw G. et al., 2006, preprint (astro-ph/0603451)
- Hirasawa T., 1969, *Prog. Theor. Phys.*, 42, 523
- Hirasawa T., Aizu K., Taketani M., 1969, *Prog. Theor. Phys.*, 41, 835
- Hutchins J. B., 1976, *ApJ*, 205, 103
- Karpas Z., Anicich V., Huntress W. T. Jr., 1979, *J. Chem. Phys.*, 70, 2877
- Kogut A. et al., 2003, *ApJS*, 148, 161
- Krstić P. S., 2002, *Phys. Rev. A*, 66, 042717
- Launay J. M., Le Dourneuf M., Zeippen C. J., 1991, *A&A*, 252, 842
- Le Bourlot J., Pineau des Forêts, G., Flower D. R., 1999, *MNRAS*, 305, 802
- Lee A. T. et al., 2001, *ApJL*, 561, L1
- Lepp S., Shull J. M., 1984, *ApJ*, 280, 465
- Lepp S., Stancil P. C., Dalgarno A., 2002, *J. Phys. B*, 35, R57
- Loeb A., Zaldarriaga M., 2004, *Phys. Rev. Lett.*, 92, 211301
- Madsen M. M., Peek J. M., 1971, *Atomic Data*, 2, 171
- Moseley J., Aberth W., Peterson J. R., 1970, *Phys. Rev. Lett.*, 24, 435
- Netterfield C. B. et al., 2002, *ApJ*, 571, 604
- Page L. et al., 2006, preprint (astro-ph/0603450)
- Palla F., Galli D., Silk J., 1995, *ApJ*, 451, 44
- Peebles P. J. E., 1968, *ApJ*, 153, 1
- Peebles P. J. E., Dicke R. H., 1968, *ApJ*, 154, 891
- Peek J. M., Hashemi-Attar A.-R., Beckel C. L., 1979, *J. Chem. Phys.*, 71, 5382
- Puy D., Alecian G., Le Bourlot J., Léorat J., Pineau des Forêts G., 1993, *A&A*, 267, 337
- Ramaker D. E., Peek J. M., 1972, *J. Phys. B*, 5, 2175
- Ramaker D. E., Peek J. M., 1973, *Atomic Data*, 5, 167
- Roberge W., Dalgarno A., 1982, *ApJ*, 255, 489
- Rybicki G. B., Dell'Antonio I. P., 1993, *ASP Conf. Ser.* 51, 548
- Saha S., Datta K. K., Barua A. K., 1978, *J. Phys. B*, 11, 3349
- Saslaw W. C., Zipoy D., 1967, *Nature*, 216, 976
- Schneider I. F., Dulieu O., Giusti-Suzor A., Roueff E., 1994, *ApJ*, 424, 983
- Seager S., Sasselov D. D., Scott D., 1999, *ApJL*, 523, L1
- Seager S., Sasselov D. D., Scott D., 2000, *ApJS*, 128, 407
- Seljak U. et al., 2005, *Phys. Rev. D*, 71, 103515
- Stancil P. C., Babb J. F., Dalgarno A., 1993, *ApJ*, 414, 672
- Stancil P. C., 1994, *ApJ*, 430, 360
- Stancil P. C., Lepp S., Dalgarno A., 1996, *ApJ*, 458, 401
- Stancil P. C., Lepp S., Dalgarno A., 1998, *ApJ*, 509, 1
- Stancil P. C., Loeb A., Zaldarriaga M., Dalgarno A., Lepp S., 2002, *ApJ*, 580, 29
- Stecher T. P., Williams D. A., 1967, *ApJ*, 149, 29
- Switzer E. R., Hirata C. M., 2005, *Phys. Rev. D*, 72, 083002
- Tegmark M., Silk J., Rees M. J., Blanchard A., Abel T., Palla F., 1997, *ApJ*, 474, 1
- Turner J., Kirby-Docken K., Dalgarno A., 1977, *ApJS*, 35, 281
- Wong W. Y., Seager S., Scott D., 2006, *MNRAS*, 367, 1666
- Yoneyama T., 1972, *Pub. Ast. Soc. Japan*, 24, 87
- Zel'dovich Y. B., Kurt V. G., Sunyaev R. A., 1968, *Zh. Eksp. Teor. Fiz.*, 55, 278
- Zygelman B., Dalgarno A., 1990, *ApJ*, 365, 239
- Zygelman B., Stancil P. C., Dalgarno A., 1998, *ApJ*, 508, 151

APPENDIX A: THE H_2^+ MOLECULAR ION

The bound states of $\text{H}_2^+(1s\sigma_g)$ are solved within the Born-Oppenheimer approximation, which for a diatomic molecular ion gives

$$\Psi(\mathbf{r}, \mathbf{R}) = \chi(\mathbf{r}|\mathbf{R}) \frac{\Phi(R)}{R} Y_{NMN}(\hat{\mathbf{R}}), \quad (\text{A1})$$

where \mathbf{r} is the electron position, \mathbf{R} is the internuclear separation vector, $\chi(\mathbf{r}|\mathbf{R})$ is the $1s\sigma_g$ electronic wavefunction, $\Phi(R)$ is the radial wavefunction, and $\hat{\mathbf{R}}$ is the unit vector in the direction of \mathbf{R} . The radial wavefunction is a solution to the Schrödinger eigenvalue equation,

$$-\frac{\hbar^2}{2\mu} \Phi''(R) + \left[V(R) + \frac{\hbar^2 N(N+1)}{2R^2} \right] \Phi(R) = E \Phi(R), \quad (\text{A2})$$

where E is the bound state energy and μ is the reduced mass of H_2^+ . The potential $V(R)$ is interpolated from the tabulated values of Bates et al. (1953) and Madsen & Peek (1971). The radiative transitions among the levels of $\text{H}_2^+(1s\sigma_g)$ are treated according to the method of Bates & Poots (1953), who give the spontaneous rates A_{ji} in terms of the wave functions² and the quadrupole moment $M(R)$ of the H_2^+ ion. The quadrupole moment is interpolated from the computations of Peek et al. (1979) for $R \leq 12a_0$, and using the asymptotic formula $M(R) \sim R^2/4 - \alpha_d a_0^3 R^{-1}$ for $R > 12a_0$ (where $\alpha_d = 9/2$ is the dipole polarizability of H).

The rate for the radiative association reaction (Eq. 4) is required for our calculation. The individual rates to and from each rotational-vibrational level of H_2^+ as a function of matter and radiation temperature are not tabulated in the literature, but can be derived using standard methods (e.g. Zygelman & Dalgarno 1990; Stancil et al. 1993). For the dipole radiative dissociation, one solves for the unbound final state Eq. (A2) using the $2p\sigma_u$ potential and the energy normalization (see e.g. Eq. 4 of Zygelman & Dalgarno 1990). Then the radiative dissociation cross section from the vN bound level with energy $E(vN) < 0$ is (Dunn 1968)

² Note that $P(R)$ in Bates & Poots (1953) is equal to our $\Phi(R)/R$.

$$\sigma_{rd}^{E1} = \frac{8\pi^3\nu}{3c} \overline{M^2}, \quad (\text{A3})$$

where $h\nu$ is the photon energy and

$$\begin{aligned} \overline{M^2} = & (2N+1)^{-1} \left[N \left| \int_0^\infty \Phi(R) D(R) f_{N-1}(R) dR \right|^2 \right. \\ & \left. + (N+1) \left| \int_0^\infty \Phi(R) D(R) f_{N+1}(R) dR \right|^2 \right]. \quad (\text{A4}) \end{aligned}$$

Here $D(R)$ is the dipole matrix element between $1s\sigma_g$ and $2p\sigma_u$ states, and $f_{N\pm 1}(R)$ are the unbound wave functions that solve Eq. (A2) with rotational quantum numbers $N \pm 1$ and energy $E(vN) + h\nu$. (Only unbound states where $N' = N \pm 1$ contribute due to dipole selection rules.) The dipole moments are interpolated from Bates (1951) and Ramaker & Peek (1973) for $R < 20a_0$, and the large- R asymptotic expression (Ramaker & Peek 1972) is used for $R \geq 20a_0$.

The net radiative dissociation rate, including both thermal and nonthermal contributions to the radiation field, is then given by integrating over all photon frequencies,

$$\begin{aligned} \beta_{vN} = & \frac{8\pi}{c^2} \int_{-E(vN)/h}^\infty \frac{\nu^2 \sigma_{rd}(\nu) d\nu}{e^{h\nu/k_B T_{CMB}} - 1} \\ & + nc \int_{-E(vN)/h}^\infty r(\nu) \sigma_{rd}(\nu) \frac{d\nu}{\nu}. \quad (\text{A5}) \end{aligned}$$

The spontaneous radiative association cross section is related to the radiative dissociation cross section by phase space factors,

$$\sigma_{ra,vN}(E) = \frac{\varpi_{\text{H}_2^+(vN)+\gamma}}{\varpi_{\text{H}+\text{H}^+}} \sigma_{rd,vN}[E - E(vN)], \quad (\text{A6})$$

where ϖ represents the number of quantum states per unit wavenumber k per unit volume for either $\text{H}_2^+(vN) + \gamma$ or $\text{H} + \text{H}^+$. These are given by

$$\varpi_{\text{H}_2^+(vN)+\gamma} = 4(2N+1)g'_{\text{nuc}} \frac{4\pi k_\gamma^2}{(2\pi)^3} \quad (\text{A7})$$

and

$$\varpi_{\text{H}+\text{H}^+} = 2 \frac{4\pi k_{\text{H}+\text{H}^+}^2}{(2\pi)^3}, \quad (\text{A8})$$

where $k_\gamma = 2\pi\nu/c$ is the photon wavenumber and $k_{\text{H}+\text{H}^+} = \sqrt{2\mu E}/\hbar$ is the relative wavenumber of H and H⁺. In addition to the usual factor $4\pi k^2/(2\pi)^3$, Eq. (A7) contains a factor of 2 from the electron spin, a factor of 2 from the photon polarization, and the nuclear spin-degeneracy factor g'_{nuc} ; Eq. (A8) contains a factor of 2 from the electron spin. The net radiative association rate coefficient to the vN level is then given by the usual integral of cross section times velocity over the Maxwell-Boltzmann distribution,

$$\begin{aligned} \alpha_{vN} = & \frac{2\sqrt{2}}{(\pi\mu)^{1/2}(k_B T_m)^{3/2}} \\ & \times \int_0^\infty E \sigma_{ra,vN}(E) e^{-E/k_B T_m} [1 + f(\nu)] dE. \quad (\text{A9}) \end{aligned}$$

Here $f(\nu)$ is the photon phase space density at frequency $\nu = [E - E(vN)]/h$, and it has been included to take into account stimulated radiative association. The phase space density from spectral distortion photons is $\ll 1$ and can be

neglected, so we approximate $f(\nu)$ by a blackbody. Substituting Eqs. (A6–A8) into Eq. (A9) then gives the final result,

$$\begin{aligned} \alpha_{vN} = & \frac{2\sqrt{2}(2N+1)g'_{\text{nuc}}h^3}{\pi^{1/2}c^2(\mu k_B T_m)^{3/2}} \\ & \times \int_{-E(vN)/h}^\infty \nu^2 \sigma_{rd}(\nu) \frac{e^{[h\nu+E(vN)]/k_B T_m}}{1 - e^{-h\nu/k_B T_{CMB}}} d\nu. \quad (\text{A10}) \end{aligned}$$

In this equation $g'_{\text{nuc}} = 1/4$ for even N and $3/4$ for odd N .